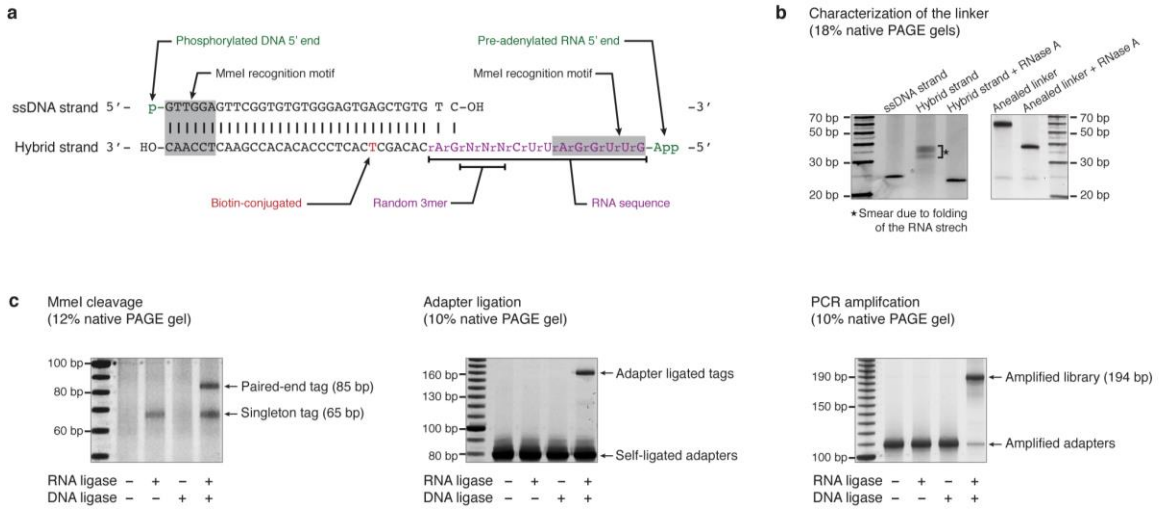

Supplementary Figure 1

Extended Data Fig. 1 | Characterization of the GRID-seq technology.

a, The design of a bivalent linker for GRID-seq. The top strand is a 5' phosphorylated DNA sequence (black) and the bottom strand consists of both DNA and RNA bases (purple) with a biotinylated T residue (red) in the middle. Randomized bases (N) served as barcodes for filtering PCR duplicates during library amplification and both ends of the linker each carry an MmeI restriction site (grey-shaded). The linker is pre-adenylated for ligation to RNA in the absence of ATP, which prevents ligation of endogenous RNAs. **b**, Characterization of the linker before (left) and after (right) annealing, showing the sensitivity of the RNA-containing linker to RNase A. **c**, Controls by omitting RNA ligase, DNA ligase or both during GRID-seq library construction, which yielded expected ligated products of singleton tags or paired-end tags (left). After adapter ligation (middle) and PCR amplification (right), the expected products were only detected after library construction with both RNA and DNA ligases.

a

Species	Samples	Raw reads	Linker-containing read pairs	Uniquely mapped read pairs (% of input)
Drosophila	S2 Rep. 1	113.7 M	95.7 M	4.5 M (4.7%)
Drosophila	S2 Rep. 2	165.7 M	74.0 M	2.0 M (2.7%)
Mixed	MDA-MB-231 + S2	46.2 M	38.7 M	–
Human	MDA-MB-231 Rep. 1	213.0 M	168.0 M	44.0 M (26.2%)
Human	MDA-MB-231 Rep. 2	294.9 M	144.8 M	40.3 M (27.8%)
Human	MM.1S Rep. 1	300.8 M	135.0 M	37.7 M (27.9%)
Human	MM.1S Rep. 2	363.6 M	149.6 M	39.2 M (26.2%)
Mouse	ESC Rep. 1	182.4 M	157.0 M	59.2 M (37.7%)
Mouse	ESC Rep. 2	130.8 M	113.6 M	44.3 M (39.0%)

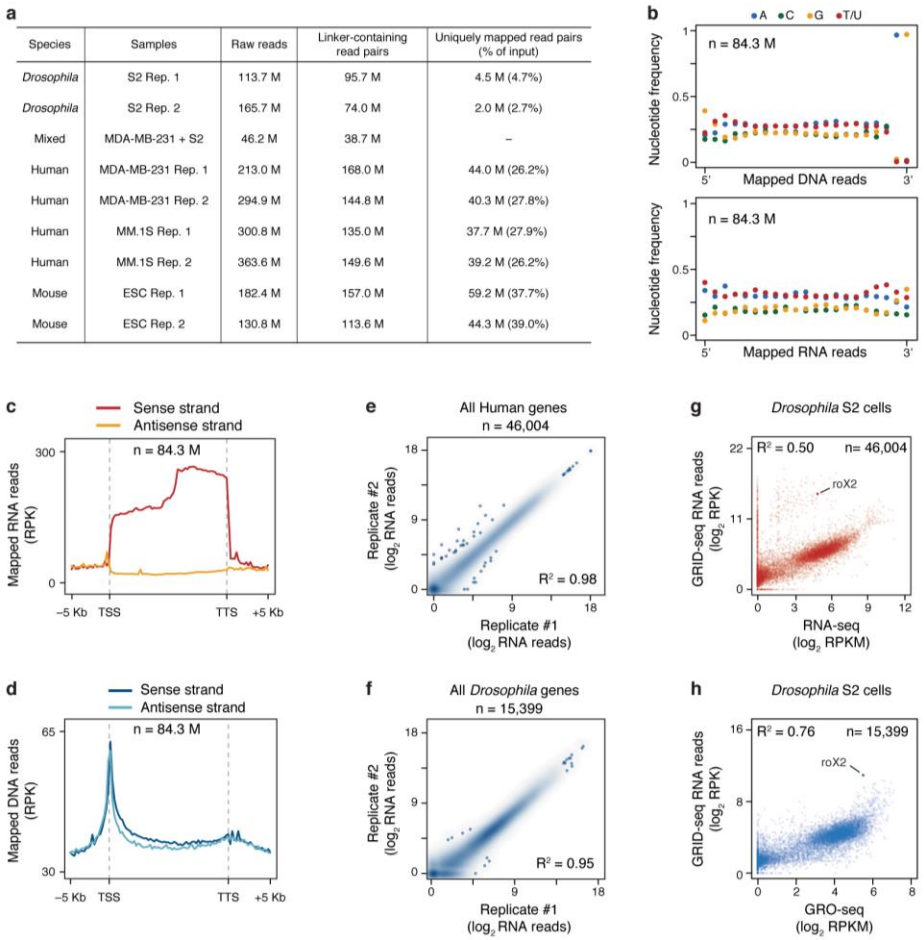

Supplementary Figure 2

Extended Data Fig. 2 | Characterization of GRID-seq libraries.

a, Summary of sequenced GRID-seq libraries constructed on two human cell lines (MDA-MB-231 and MM.1S), one mESC, and one *Drosophila* S2 cells. Shown are raw reads, linker-containing reads, and uniquely mapped reads from mated RNA/DNA pairs. **b**, Nucleotide frequency of DNA (up) and RNA (bottom) reads. Note specific dinucleotide as part of the AluI recognition site at the 3' end of DNA reads, but the lack of nucleotide bias in any position of RNA reads. **c**,**d**, Strand orientation of mapped RNA (c) and DNA (d) reads. Note the same strand orientation of mapped RNA reads as their transcripts, but not DNA. **e**,**f**, Reproducibility of GRID-seq libraries constructed on human (e) and *Drosophila* (f) cells. **g**,**h**, Comparison of GRID-seq detected RNA reads with gene expression detected by RNA-seq of rRNA-depleted total RNA (g) or GRO-seq (h) in *Drosophila* S2 cells. The lncRNA roX2 is highlighted in both plots. RPK: GRID-seq reads per Kb. RPKM: reads per Kb per million mapped reads.

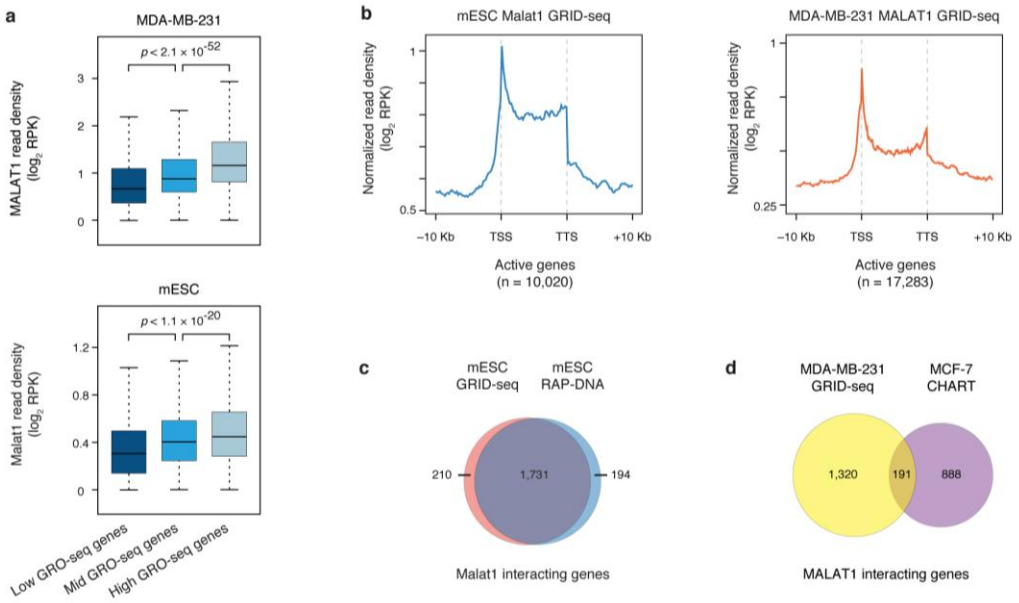

Supplementary Figure 3

Extended Data Fig. 3 | Characteristics of MALAT1 interaction with chromatin in human and mouse cells.

a, MDA-MB-231 cells (upper panel) and mESCs (bottom panel). **b**, Meta-analysis of MALAT1-chromatin interactions in human (left panel) and mouse (right panel) cells on a composite gene model. TSS: Transcription Start Site. TTS: Transcription Termination Site. **c**, Comparison of MALAT1-chromatin interactions detected by GRID-seq versus RAP-DNA in mESCs. **d**, Comparison of MALAT1-chromatin interactions detected by GRID-seq in MDA-MB-231 cells versus those identified by CHART in MCF-7 cells. Note that these meta-analysis plots were based on the data before background correction, which remained the same after background subtraction. *P*-values in a, c, and d were determined by Fisher's exact test.

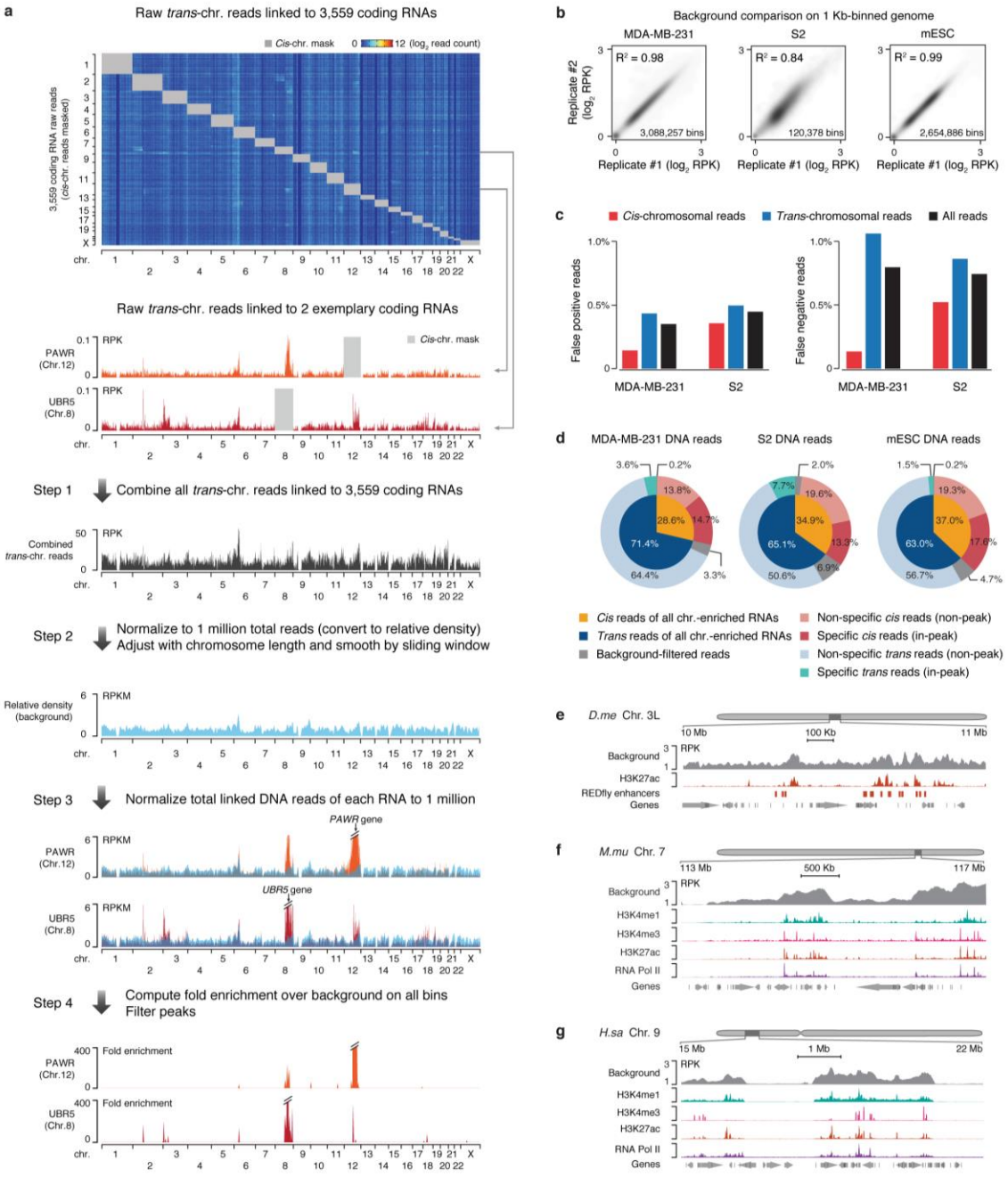

Supplementary Figure 4

Extended Data Fig. 4 | Construction of a background model for GRID-seq data analysis.

a, Steps in building the background with *trans*-chromosomal interacting mRNAs. GRID-seq detected raw DNA reads of *trans*-acting mRNAs (n=3,559) on chromatin were displayed on all chromosomes with their *cis*-acting signals masked by grey boxes. Two specific mRNAs on their *trans* locations were highlighted below the heatmap. Step 1: All *trans*-acting mRNAs were summed, and then in Step 2, normalized to 1 million total reads. Step 3: The GRID-seq signals of the two specific mRNAs were similarly normalized to 1 million across all chromosomes. Red signals above the general background were highlighted. Step 4: Specific interaction sites were displayed after background correction. **b**, Comparison of deduced background from replicate GRID-seq

libraries constructed on human MDA-MB-231 cells, mESCs and *Drosophila* S2 cells. Each genome was 1 Kb binned for global comparison. RPK: reads per Kb. **c**, Comparison between the true background based on the human-*Drosophila* mixing experiment and the deduced background from mRNA *trans*-chromosomal reads in inferring specific RNA-chromatin interactions. The data illustrate <1% discrepancies in inferring *cis*, *tran*s, or all reads in both MDA-MB-231 and S2 datasets. **d,** Quantification of *cis* and *trans*-chromosomal reads distribution before and after background correction. **e**,**f**,**g**, Background GRID-seq signals in open chromatin regions in human (e), mouse (f), and *Drosophila* (g) cells. Chromatin marks and RNA Pol II binding were displayed on autoscale.

Nature Biotechnology: doi:10.1038/nbt.3968

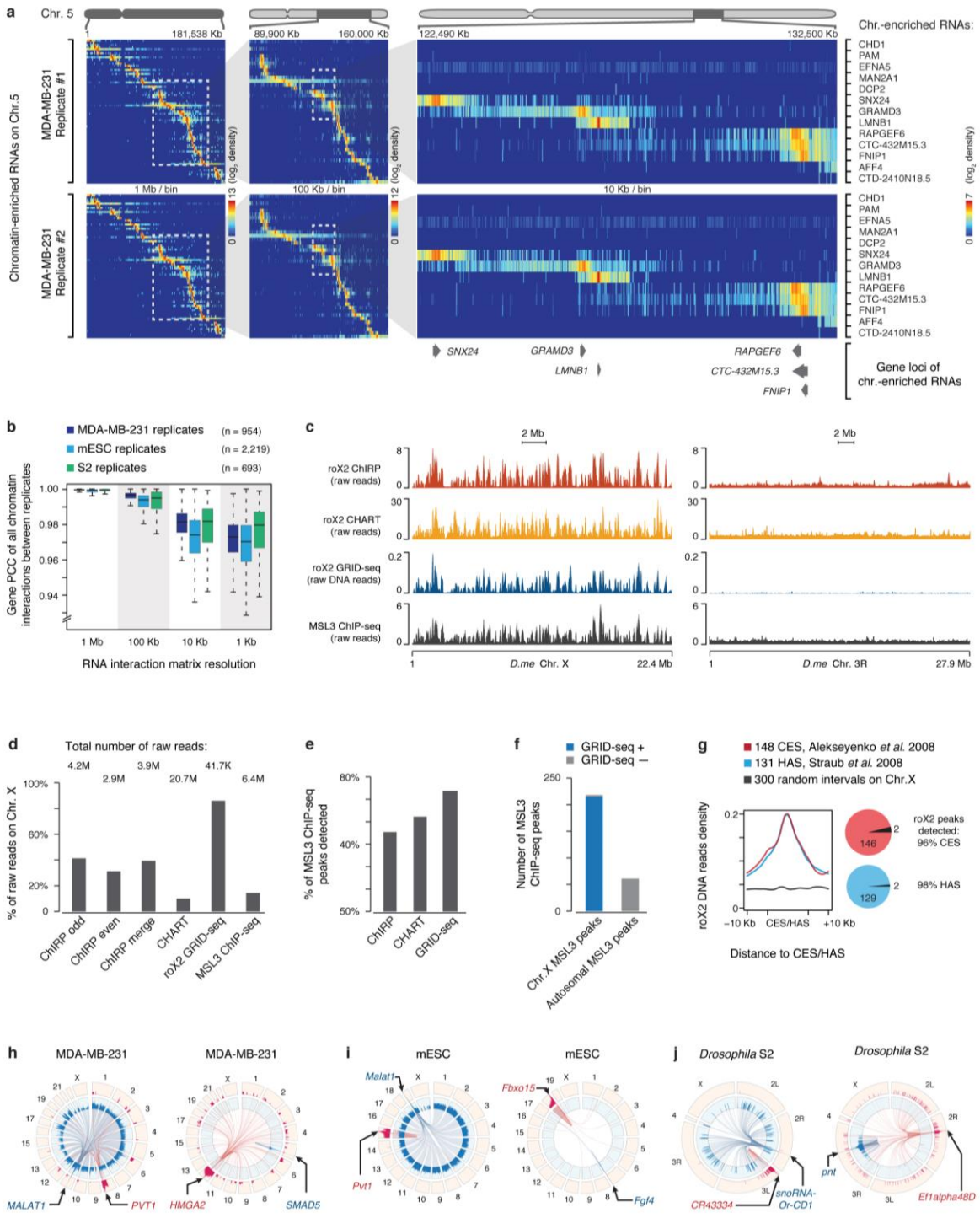

Supplementary Figure 5

Extended Data Fig. 5 | Characteristics of RNA-chromatin interactions.

a, RNA-chromatin interaction heatmaps on Chr. 5 constructed from two independent GRID-seq libraries on MDA-MB-231 cells. Boxed regions in each panel were enlarged with increasing resolution in the next panel on the right. A set of representative chromatin-enriched RNAs are labeled on the right and their encoding gene loci illustrated on the bottom. **b**, Pearson's Correlation Coefficient of GRID-seq interaction density of each RNA at

increasing resolution (decreasing bin size) across genomes between the replicates performed on MDA-MB-231 cells, mESC and *Drosophila* S2 cells. **c,** Whole chromosome view of raw roX2 GRID-seq DNA reads on *Drosophila* Chr. X and Chr. 3R in comparison with raw signals detected by ChIRP and CHART, as well as ChIP-seq signals for the roX2 binding protein MSL3. **d,** Percentage of total raw roX2 GRID-seq DNA reads on Chr. X in comparison with the raw data of ChIRP, CHART, GRID-seq and MSL3 ChIP-seq. Total number of raw read for each dataset is noted on top of each bar. **e**, Comparison of roX2 peaks identified by ChIRP, CHART, and GRID-seq with MSL3 ChIP-seq peaks in *Drosophila* S2 cells, showing the highest overlap between GRID-seq and MSL3 ChIP-seq identified peaks. **f**, Comparison of GRID-seq identified roX2 peaks with MSL3 ChIP-seq peaks on Chr. X and autosomes, showing their overlap only on Chr. X. **g,** Meta-analysis of roX2 GRID-seq DNA reads relative to chromatin binding of CES and HAS. Pie charts on the right illustrate the overlaps between CES/HAS peaks and roX2 GRID-seq peaks. **h**,**i**,**j**, Circos plots depicting chromatin-interactions of two representing lncRNAs (left panels) and two protein-coding mRNAs (right panels) in each cell type. In MDA-MB-231 cells (h), the lncRNA MALAT1 broadly interacted with all chromosomal regions whereas PVT1 was predominantly involved in local and cis-chromosomal interactions, although trans-chromosomal interaction signals were also evident in various specific locations (h, left panel). Similarly, RNAs from the coding HMGA2 gene showed chromatin interactions in local, *cis* and *trans* modes whereas RNAs from the coding SMAD5 gene was largely confined in local interactions (h, right panel). Similar examples also illustrated distinct chromatin interaction patterns with both coding RNAs and lncRNAs in mESC (i) and *Drosophila* S2 cells (j).

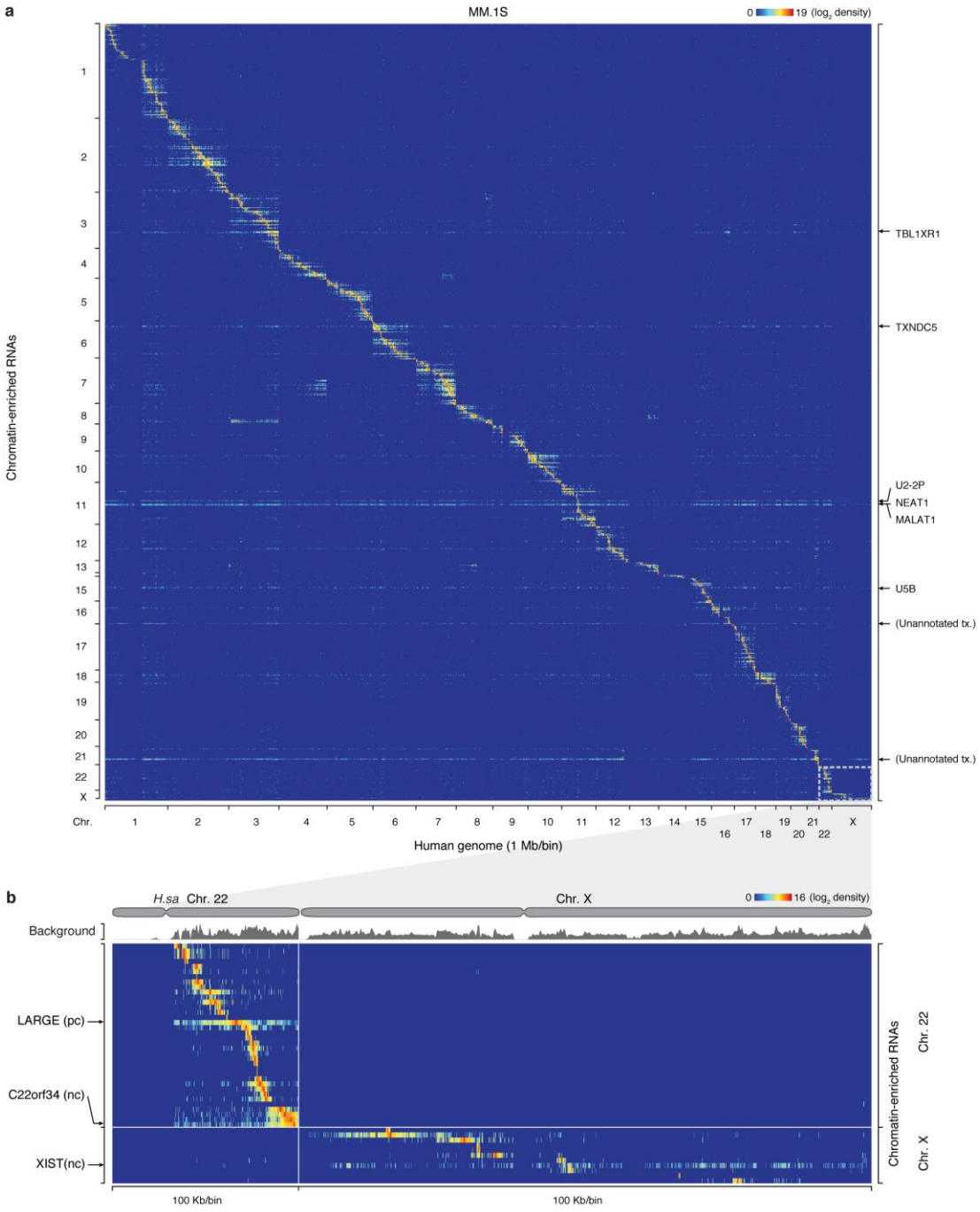

Supplementary Figure 6

Extended Data Fig. 6 | Global view of RNA-chromatin interactions in human MM.1S cells.
a, Heatmap showing RNA-chromatin interactions across the whole human genome in MM.1S cells. Row: chromatin-enriched RNAs. Column: human genome in 1 Mb resolution. Representative *trans*-chromosomal interacting RNAs are labeled on the right. **b**, Enlarged heatmaps of boxed Chr. 22 and X in a, showing detailed RNA-chromatin interactions on Chr. 22 (left) and Chr. X (right). Representative RNAs are labeled on the left (pc: protein-coding RNAs, nc: non-coding RNAs), highlighting the non-coding RNA XIST on Chr. X (note that

XIST is expressed in MM.1S cells, but not in MDA-MB-231 cells). Top: The background deduced from endogenous traveling mRNAs.

Nature Biotechnology: doi:10.1038/nbt.3968

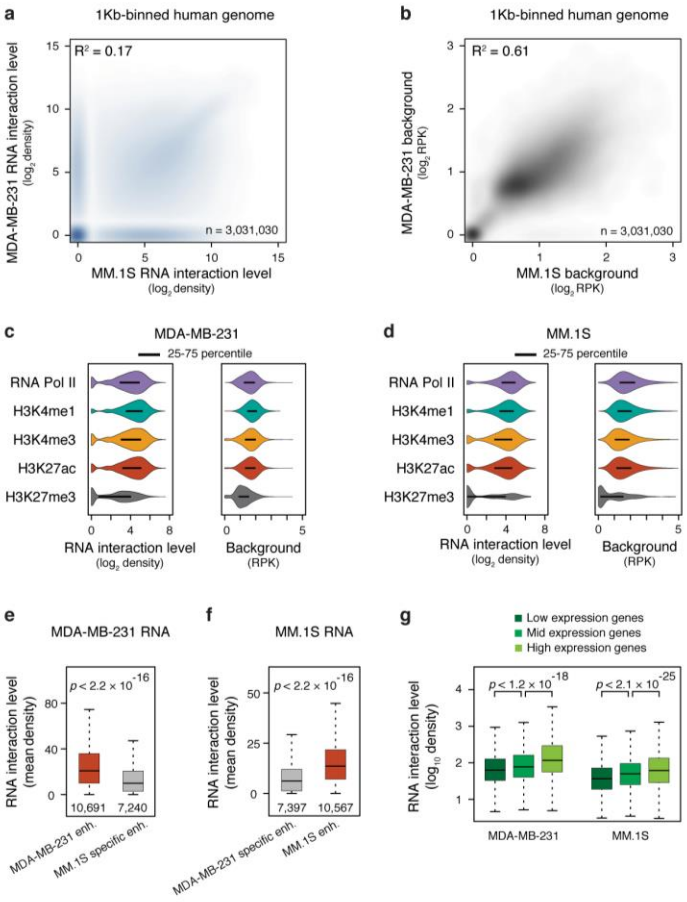

Supplementary Figure 7

Extended Data Fig. 7 | RNA-chromatin interactions on cell type-specific enhancers.
a,b, Scatterplots of foreground (a) and background (b) of GRID-seq signals between MDA-MB-231 and MM.1S cells in the 1 Kb-binned human genome. **c**,**d**, Violin plots showing co-enrichment of specific RNA-chromatin interactions and key chromatin features in MDA-MB-231 cells (c) and MM.1S (d). Left: Enrichment of mean chromatin interaction signals of GRID-seq RNA density after background correction relative to ChIP-seq peaks of RNA Pol II, H3K4me1, H3K4me3, H3K27ac and H3K27me3. Right: Background signals. RPK: reads per Kb. Bars represent the range from 25 to 75 percentiles. **e**,**f**, Quantification of RNA-chromatin interaction levels on enhancers in the same cell type (orange) relative to specific enhancers in a different cell type (grey). **g**, Correlation of RNA-chromatin interaction levels on promoters with gene expression in MDA-MB-231 and MM.1S cells.

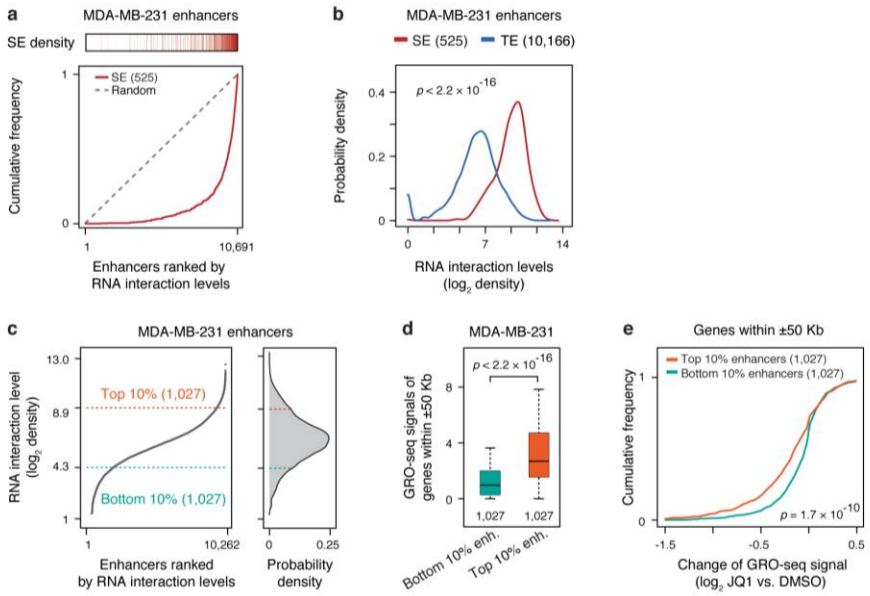

Supplementary Figure 8

Extended Data Fig. 8 | RNA interaction levels on super-enhancers and relative contribution of typical and super-enhancers to transcription.

a, Super-enhancers in relationship to RNA-chromatin interaction levels. Enhancers in MDA-MB-231 cells were ranked by RNA interaction levels. Each red bar on top represents a super-enhancer. Red curve: The accumulative curve of rank-ordered RNA-chromatin interactions; Grey dashed line: Random distribution. **b**, Density distribution of chromatin-enriched RNAs at super-enhancers (SE, red) and typical enhancers (TE, blue). **c**, Left: Rank-ordered RNA-chromatin interaction levels at all active enhancers. Right: The Top 10% and bottom 10% enhancers with the most and the least RNA interactions, respectively, selected for functional analysis. **d**, Gene transcription associated with top 10% enhancers (orange box) and bottom 10% enhancers (green box). **e**, Accumulation curves of transcription changes of genes associated with top 10% and bottom 10% enhancers in response to JQ1 treatment in MDA-MB-231 cells. Statistical significance of comparison is estimated by Student's t-test in panel b, d and e.

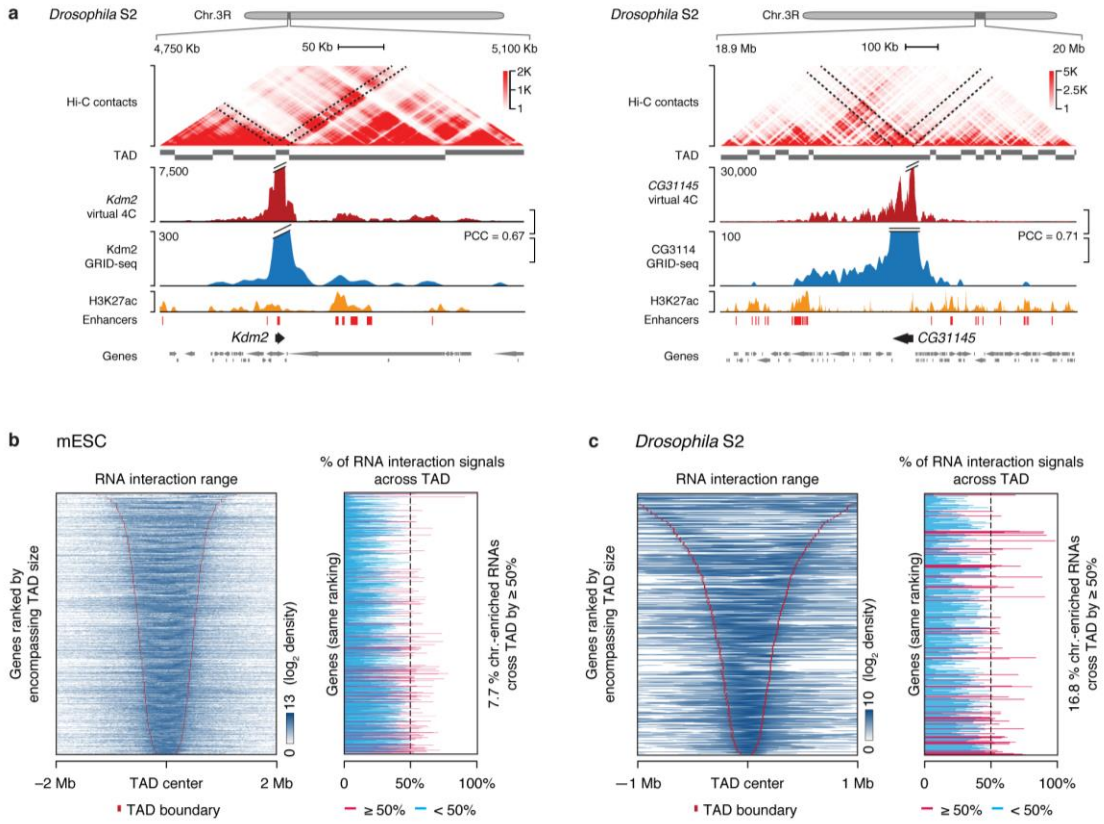

Supplementary Figure 9

Extended Data Fig. 9 | Comparison between Hi-C and GRID-seq in different cell types.
a, Examples of Hi-C interactions in comparison with GRID-seq detected RNA interactions relative to previously assigned TADs in *Drosophila* S2 cells. H3K27ac ChIP-chip signals and reporter scored enhancers from the RedFly database were displayed at bottom. **b**,**c**, Left panels: GRID-seq signals relative established TADs in mESCs (b) and *Drosophila* S2 cells (c). Right panels: GRID-seq signals across TAD boundaries. Red lines indicate chromatin-enriched RNAs with more than 50% GRID-seq signals spread to adjacent TADs.

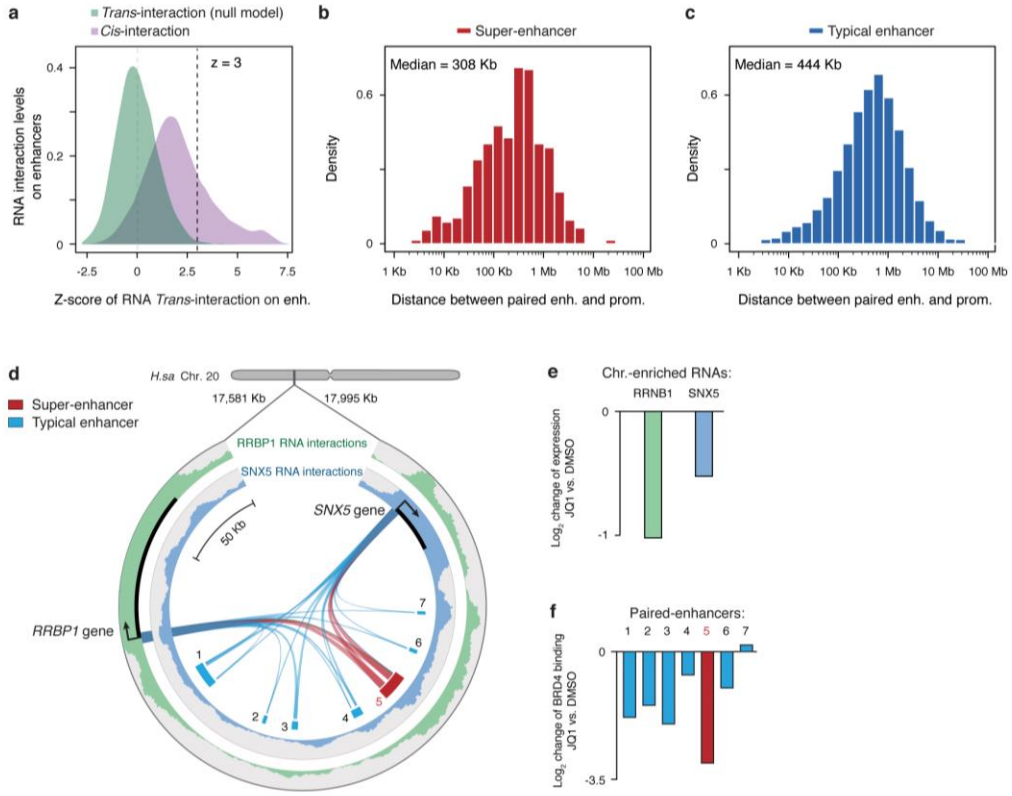

Supplementary Figure 10

Extended Data Fig. 10 | Inferred enhancer-promoter distance and examples.

a, Density distributions of *cis*- and *trans*-chromosomal RNA interaction levels on enhancers in MM.1S cells. x-axis: Z-scores of all *trans*-chromosomal RNA interactions (green). Z≥3 was used to identify significant RNA interactions on individual promoter and enhancer elements. **b**,**c**, Distribution of linear DNA distance between genes and RNA decorated super-enhancers (b) and typical enhancers (c). **d**, Circos plot, showing a representative case of two chromatin-enriched RNAs RRBP1 and SNX5 on nearby seven enhancers, one of which corresponds to a super-enhancer (red) in MM.1S cells. The RRBP1 RNA interaction profile is shown on the outer track (green) and the SNX5 RNA interaction profile on the inter track (blue). Ribbons connecting with enhancers illustrate inferred enhancer-promoter association. **e**, **f**, Upon JQ1 treatment, fold-changes in gene expression are shown in e and fold-changes in BRD4 binding on individual enhancers in f.